

Response to the comments by the reviewers
Qingcai Chen, Haoyao Sun and Yanlin Zhang.

We appreciate the comments from editor and the reviewers. We have answered the supplementary comments and improved the sentence expression of the article. We look forward to the successful publication of this article.

Our responses to the comments from the reviewers and changes made in the paper are listed below.

The authors have done a good job responding to the referee's comments. There remain a few points where some clarification or correction is needed.

We appreciate the positive evaluation of this work.

Specific comments:

(1) In their response to Reviewer #1 concerning Section 2.2, the authors say "Cut the sample filter into thin strips". It would be much better if they said "The filters were cut into thin strips".

We appreciate this comment from the reviewer. We have modified this part as follows:

L105-107: The filters were cut into thin strips (5 mm × 28 mm), and put it into the sample tank of the quartz tissue cell (the size of the sample tank is 10 mm × 30 mm).

(2) In their response to Reviewer #1 concerning Section 2.3, It is not clear what is meant by "qualified ions".

We appreciate this comment from the reviewer. Qualified ions here refers to the typical ion fragments of each PAHs, which was used to determine the type of PAHs. We have provided another reference that describes the PAHs analysis in detail (Song et al., 2020). In addition, we also changed the expression about this point as follows:

L134-136: Sixteen target PAHs were identified based on retention time and typical ion fragments of each PAH standards, including 16 EPA parent PAHs (p-PAHs).

L141-142: Specific testing protocols have been described previously (Han et al., 2018; Song et al., 2020).

Song, W., Cao F., Lin Y., Haque, M. M., Wu, X., Zhang, Y., Zhang, C., Xie, F., Zhang Y., 2020. Extremely high abundance of polycyclic aromatic hydrocarbons in aerosols from a typical coal-combustion rural site in China: Size distribution, source identification and cancer risk assessment. Atmos. Res. 248, 105192.

(3) The response that explains the g-factor: Instead of “using EPR to detect the sample”, it would be more correct to say “using EPR to analyze the sample”. This phrase appears in several places, so should be corrected everywhere.

We appreciate this comment from the reviewer. We have modified this section as follows:

L221-222: The g-factor obtained by using EPR to analyze the sample is an important parameter to distinguish the type of EPFR.

(4) The response to the Reviewer’s question on L204-206, the authors have still not specified if the percentages were by mass.

We appreciate this comment from the reviewer. It is not the contribution by PM mass but is the concentration of EPFRs. We have modified this section as follows:

L205-206: Figure 1b shows the concentration ratio of EPFRs in coarse and fine particles. The contribution of EPFRs in fine PM in summer is only 14.9%, while in winter is 58.5%.

(5) The authors response L220-242. The phrase “the variation in the g-factor with concentration in different season is different.” Is a bit awkward, it would be better to simply say “the g-factor varied differently depending on season”.

We appreciate this comment from the reviewer. We have modified this section as follows:

L235-236: As shown in Figure 2b, the g-factor varied differently depending on season.

(6) The response to Comment (7). What is “the catering process”?

We appreciate this comment from the reviewer. The catering process refers to the process of cooking, mainly including cooking fume and the process of burning biomass on stoves in rural areas.

(7) Line 24 , Instead of “other fuel combustions” , just say “other fuels”

We appreciate this comment from the reviewer. We have modified this section as follows:

L24: ...while other fuels are the major source in summer.

(8) Line 159. The phrase that was changed is better, but should be changed to the past tense. “A gradient-based multiplication algorithm was used to find a solution..... and then the first algorithm was used..... based on the least-squares effective-set algorithm.”

We appreciate this comment from the reviewer. We have modified this section as follows:

L154-157: A gradient-based multiplication algorithm was used to find a solution from multiple random starting values, and then the first algorithm was used to find the final solution based on the least-squares effective-set algorithm.

1 **Size-resolved exposure risk of persistent free radicals (PFRs)**
2 **in atmospheric aerosols and their potential sources**

3 Qingcai Chen,^a Haoyao Sun,^a Wenhui Song,^b Fang Cao,^b Chongguo Tian,^c Yan-Lin
4 Zhang^{b*}

5 ^a *School of Environmental Science and Engineering, Shaanxi University of Science and*
6 *Technology, Xi'an 710021, China*

7 ^b *Yale–NUIST Center on Atmospheric Environment, International Joint Laboratory on Climate*
8 *and Environment Change (ILCEC), Nanjing University of Information Science and Technology,*
9 *Nanjing 210044, China*

10 ^c *Key Laboratory of Coastal Environmental Processes and Ecological Remediation, Yantai*
11 *Institute of Coastal Zone Research, Chinese Academy of Sciences, Yantai, 264003, China*

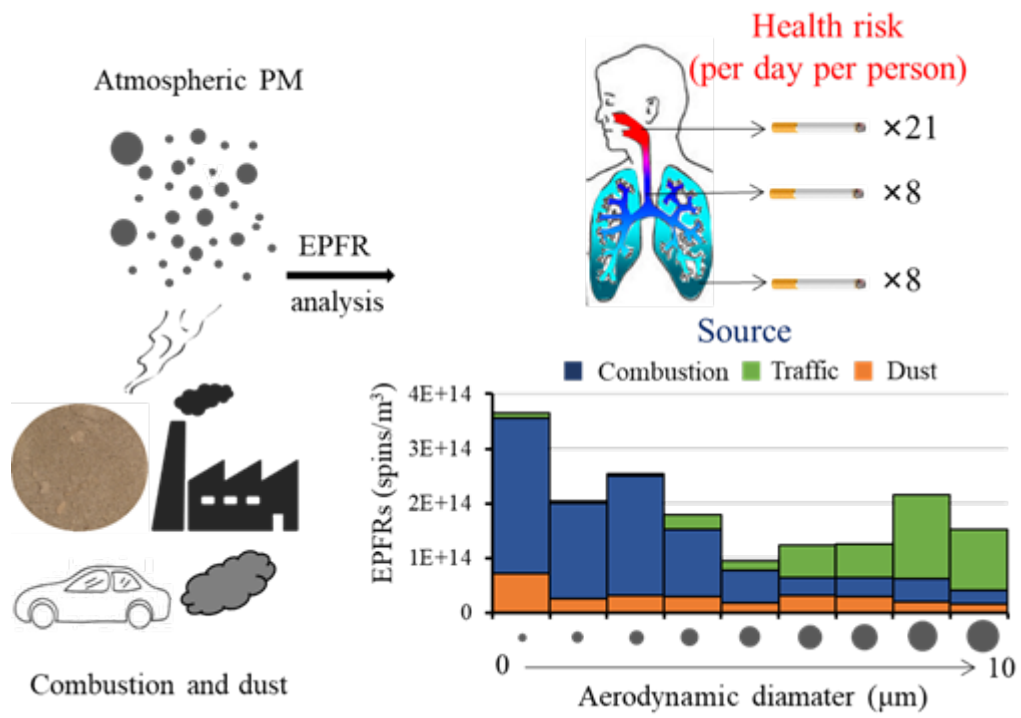
12 *Corresponding Author at: Ningliu Road 219, Nanjing 210044, China.

13 *E-mail address: dryanlinzhang@outlook.com or zhangyanlin@nuist.edu.cn (Yan-Lin Zhang).*

14 **Abstract:** Environmentally persistent free radicals (EPFRs) are a new type of
15 substance with potential health risks. EPFRs are widely present in atmospheric
16 particulates, but there is a limited understanding of the size-resolved health risks of
17 these radicals. This study reports the exposure risks and source of EPFRs in
18 atmospheric particulate matter (PM) of different particle sizes ($<10\ \mu\text{m}$) in Linfen, a
19 typical coal-burning city in China. The type of EPFRs in fine particles ($< 2.1\ \mu\text{m}$) is
20 different from that in coarse particles ($2.1\text{-}10\ \mu\text{m}$) in both winter and summer.
21 However, the EPFR concentration is higher in coarse particles than in fine particles in
22 summer, and the opposite trend is found in winter. In both seasons, combustion
23 sources are the main sources of EPFRs with coal combustion as the major contributor
24 in winter, while other fuel-combustions are the major source in summer. Dust
25 contributes part of the EPFRs and it is mainly present in coarse particles in winter and
26 the opposite in summer. The upper respiratory tract was found to be the area with the
27 highest risk of exposure to EPFRs of the studied aerosols, with an exposure equivalent
28 to that of approximately 21 cigarettes per person per day. Alveolar exposure to EPFRs
29 is equivalent to 8 cigarettes per person per day, with combustion sources contributing
30 the most to EPFRs in the alveoli. This study helps us to better understand the potential
31 health risks of atmospheric PM with different particle sizes.

32 **Key words:** EPFRs; particle size distribution; source; generation process

33



36 **1. Introduction**

37 Free radicals are atoms or groups containing unpaired electrons, such as hydroxyl
38 radicals and superoxide radicals, and they usually have strong chemical reactivity and
39 short lifetimes (Pryor et al., 1986; Finkelstein., 1982). Free radicals with long
40 lifetimes (months or even years) in the environment are currently called
41 environmentally persistent free radicals (EPFRs), which have received much attention
42 in recent years as new environmentally hazardous substances (Vejerano et al., 2018;
43 Gehling, 2013; Chen et al., 2019c). EPFRs can be used as an active intermediate to
44 catalyze the production of reactive oxygen species (ROS) by oxygen molecules, thus
45 endangering human health (D'Arienzo et al., 2017; Thevenot et al., 2013; Harmon et
46 al., 2018; Blakley et al., 2001; Khachatryan et al., 2011). Studies have found that
47 EPFRs are present in different environmental media, such as water and soil, and even
48 in the atmosphere (Dellinger et al., 2001; Truong et al., 2010; Vejerano et al., 2012).

49 A number of studies have investigated the occurrences, sources and formation
50 process of EPFRs in atmospheric particulates in different regions. For example, in the
51 studies of Rostock in Germany, Taif in Saudi Arabia and Xuanwei in China, the
52 average concentration of EPFRs in atmospheric particulate matter (PM) was reported
53 to be in the range of $\sim 10^{16}$ - 10^{18} spins/g (Wang et al., 2018; Arangio et al., 2016;
54 Shaltout et al., 2015). Atmospheric EPFRs are mainly carbon-centered radicals with
55 adjacent oxygen atoms (Gehling et al., 2013). EPFRs of different lifetimes are present
56 in atmospheric PM, with only a few hours for short-lifetime EPFRs and several years
57 for long-lifetime EPFRs that show no signs of decay (Gehling et al., 2013; Chen et al.,
58 2019c). Most studies indicate that sources of transportation and combustion may be
59 the primary EPFR sources in atmospheric PM (Wang et al., 2018; Yang et al., 2017;
60 Chen et al., 2019b). Chen et al. (2018b and 2019b) found that strong atmospheric
61 photochemical effects in summer and dust particles may also be important sources of
62 EPFRs. The process of electron transfer and stabilization between the surface of metal
63 oxides (such as iron, copper, zinc and nickel) and substituted aromatic molecules

64 under high temperatures is considered to be the main process for the formation of
65 EPFRs in atmospheric particles (Truong., 2010; Vejerano et al., 2012a; Patterson et al.,
66 2013; Vejerano., 2010; Vejerano et al., 2012b). However, the study by Chen et al.
67 (2018a) suggests that EPFRs in atmospheric particulates are mainly derived from
68 graphite oxide-like substances produced during combustion. In addition to primary
69 sources such as combustion, secondary chemical processes in the atmosphere may
70 also be an important source of EPFRs in atmospheric PM (Chen et al. 2019b and
71 2019d; Tong et al., 2018).

72 Different particle sizes of atmospheric PM pose different health risks to humans,
73 depending on the deposition efficiency of the particles and the chemical composition
74 and concentrations of hazardous substances they contain (Strak et al., 2012;
75 Valavanidis et al., 2008). Among various hazardous substances, EPFRs may also be
76 involved in the toxicity of atmospheric particulates. Yang et al. (2017) studied the the
77 EPFRs that are extractable by dichloromethane in different particle sizes in Beijing in
78 winter and found that the concentration of EPFRs was the highest in particles with
79 sizes $< 1 \mu\text{m}$. Arangio et al. (2016) found that the concentration of EPFRs in 180 nm
80 particles was the highest in the 56 nm - 1.8 μm particle size range. Although several
81 studies have examined the particle size distribution of EPFRs, systematic studies have
82 not been conducted on the formation process, source and exposure assessment of
83 EPFRs in atmospheric particles with different particle sizes.

84 This study takes Linfen as an example. Linfen is one of the cities in China with
85 the most serious air pollution and is a typical coal-burning city. The particle size
86 distribution of EPFRs in atmospheric PM in this region was studied by EPR
87 spectrometry. The effects of particle size and season on the source, formation process,
88 and health risk of EPFRs were revealed. In particular, the comprehensive health risks
89 of EPFRs were evaluated, and it was found that the upper respiratory tract is the area
90 with the highest risk of EPFRs exposure, which is equivalent to twenty-one cigarettes
91 per person per day. This study is of great significance for understanding the source
92 and formation process of EPFRs in atmospheric particulates as well as for health risk

93 assessments.

94 **2. Experimental section**

95 *2.1 Sample collection*

96 The sampling site for this study is located in Hongdong (36°23', 111°40'E) in
97 Shanxi, China. To collect atmospheric particles of different sizes (0-10 μm), this study
98 used a Thermo-Anderson Mark II sampler to collect aerosol samples of 9 sizes. The
99 samples were collected on a prebaked quartz filter (450 °C, 4.5 hours), and the
100 sampling dates were as follows: in winter, January 26 to February 4, 2017, $n = 10$; and
101 in summer, July 31 to August 24, 2017, $n = 12$. The samples were placed in a -20 °C
102 refrigerator prior to analysis.

103 *2.2 EPFR analysis*

104 The EPR spectrometer (MS5000, Freiberg, Germany) is used to detect EPFRs in
105 atmospheric samples. ~~The filters were cut into thin strips~~ Cut the sample filter into thin
106 strips (5 mm \times 28 mm), and put it into the sample tank of the quartz tissue cell (the
107 size of the sample tank is 10 mm \times 30 mm). Then the quartz tissue cell with attached
108 filter sample was placed in a resonant cavity and analyzed by an EPR spectrometer.
109 The detection parameters were magnetic field strength, 335 - 342 mT; detection time,
110 60 s; modulation amplitude, 0.20 mT; number of detections, 1; and microwave
111 intensity, 8.0 mW. Specific testing protocols have been described previously (Chen et
112 al., 2018c).

113 *2.3 Carbon composition analysis*

114 The contents of organic carbon (OC) and elemental carbon (EC) in the filter
115 samples were analyzed using a semicontinuous OC/EC analyzer (Model 4, Sunset Lab.
116 Inc., Oregon, USA) with a NIOSH 5040 detection protocol (Lin et al., 2009).

117 The water-soluble organic carbon (WSOC) concentration was analyzed using an
118 automatic TOC-LCPH analyzer (Shimadzu, Japan). The WSOC extraction was

119 performed with ultrapure water under ultrasonication for 15 minutes, and all WSOC
120 concentrations were blank corrected. The concentration of OC in the MSM
121 (Methanol-soluble materials) was calculated as the difference between the OC and
122 WSOC (Water-soluble organic carbon) concentrations. This calculation assumes that
123 all water-insoluble organic carbon (WISOC) in the aerosol can be extracted with
124 MeOH, and the rationality of this assumption has been verified elsewhere (Mihara et
125 al., 2011; Liu et al., 2013; Cheng et al., 2016; Chen et al., 2019a).

126 *2.4 PAH analysis*

127 PAHs were detected using gas chromatography/mass spectrometry (GC/MS) on a
128 GC7890B/MS5977A (Agilent Technologies, Clara, CA). Quartz-fiber filter samples
129 (8 mm in diameter) were cut from each 25-mm quartz-fiber filter substrates used on
130 the ELPI impactor stages using a stainless-steel round punch over a clean glass dish
131 and loaded into the TD glass tube. Next, the TD glass tube was heated to 310 °C at a
132 rate of 12 °C/min and thermally desorbed at 310 °C for 3 min. The desorbed organic
133 compounds were trapped on the head of a GC-column (DB-5MS: 5% diphenyl-95%
134 dimethyl siloxane copolymer stationary phase, 0.25-mm i.d., 30-m length, and
135 0.25-mm thickness). Sixteen target PAHs were identified based on retention time and
136 [typical ion fragments of each PAH standards](#)~~qualified ions of the standards~~, including
137 16 EPA parent PAHs (p-PAHs). The method detection limits (MDLs) ranged from 0.2
138 pg/mm² (Ace) to 0.6 pg/mm² (Incdp). Naphthalene-D8, acenaphthene-D10,
139 phenanthrene-D10, chrysene-D12, and perylene D12 were used for the analytical
140 recovery check. All compounds were recovered with a desorption recovery percentage
141 of > 90%. Specific testing protocols have been described previously (Han et al., 2018;
142 [Song et al., 2020](#)).

143 *2.5 Metal element analysis*

144 The concentration of metal elements in the samples was determined by a Thermo
145 X2 series inductively coupled plasma mass spectrometer (ICP-MS, Thermo, USA).
146 The metal elements analyzed in summer were Na, Mg, K, Ca, Ti, V, Cr, Mn, Fe, Co,

147 Ni, Cu, Zn, As, Cd, Pb, and Al, and those in winter were Al, Zn, V, Cr, Mn, Co, Ni, Cu,
148 As, Se, Sr, Cd, Ba, and Pb. The specific measurement method is based on the study of
149 Qi et al (2016).

150 2.6. Data statistics method

151 The source and formation process of EPFRs in PM with different particle sizes
152 were analyzed by nonnegative matrix factorization (NMF). The method is based on
153 the study of Chen et al (2016 and 2019e). Briefly, NMF analysis of EPFR data, metal
154 element contents, OC/EC contents and PAH contents was performed in MATLAB.
155 The version of the NMF toolbox is 1.4 (<https://sites.google.com/site/nmftool/>). A
156 gradient-based multiplication algorithm was used to find a solution from multiple
157 random starting values, and then the first algorithm was used to find the final solution
158 based on the least-squares effective-set algorithm~~Use the gradient-based~~
159 ~~multiplication algorithm to find a solution from multiple random starting values, and~~
160 ~~then use the first algorithm to find the final solution based on the least squares~~
161 ~~effective-set algorithm~~. To find a global solution, the model was run 100 times, each
162 time with a different initial value. By comparing the 1-12 factor model (Figure S4)
163 with the residual of the spectral load, the 6 factor (summer) and 10 factor (winter)
164 NMF models were finally selected.

165 2.7. EPFR exposure evaluation

166 To assess the health risks of EPFRs, this study divided the respiratory system into
167 three parts based on the human breathing model: extrathoracic (ET) areas, including
168 the anterior nasal cavity, posterior nasal cavity, oral cavity, and throat;
169 tracheobronchial (TB) areas, including the trachea, bronchi, bronchioles, and terminal
170 bronchi; and pulmonary (P) areas, including the alveolar ducts and alveoli. Then, the
171 sedimentation rates of different particle sizes in different areas of the respiratory
172 system were determined to calculate the exposure risk of EPFRs. Here, the human
173 respiratory system particulate deposition model of Salma et al. (2002) was used, and
174 the specific data can be found in Table S3 and S4.

175 In addition, the daily inhaled concentration of EPFRs into the concentration of free
176 radicals in cigarettes were converted. The specific conversion method is as follows:

$$177 \quad N_{\text{cig}} = (C_{\text{EPFRs}} \cdot V) / (RC_{\text{cig}} \cdot C_{\text{tar}}) \quad (1)$$

178 where N_{cig} represents the number of cigarettes (/person/day), C_{EPFRs} (spins/m^3)
179 represents the atmospheric concentration of EPFRs in PM, and V represents the
180 amount of air inhaled by an adult per day ($20 \text{ m}^3/\text{day}$) (Environmental Protection
181 Agency, 1988). RC_{cig} ($4.75 \times 10^{16} \text{ spins}/\text{g}$) (Baum et al., 2003; Blakley et al., 2001;
182 Pryor et al., 1983; Valavanidis and Haralambous, 2001) indicates the concentration of
183 free radicals in cigarette tar, and C_{tar} ($0.013 \text{ g}/\text{cig}$) indicates the amount of tar per
184 cigarette (Gehling et al., 2013).

185 **3. Results and discussion**

186 *3.1 Concentrations and types of EPFRs*

187 Figure 1a shows the concentration distribution of EPFRs with different particle
188 sizes in different seasons. EPFRs were detected in the particles of each tested size (the
189 EPR spectrum is shown in Figure S1), but their EPFR concentration levels were
190 different. In summer, the concentration of EPFRs in fine particles (particle size < 2.1
191 μm) is $(3.2 - 8.1) \times 10^{13} \text{ spins}/\text{m}^3$, while the concentration of EPFRs in coarse
192 particles (particle size $> 2.1 \mu\text{m}$) is 1-2 orders of magnitude higher than that of fine
193 particles, reaching values of $(2.2 - 3.5) \times 10^{14} \text{ spins}/\text{m}^3$. Winter samples show
194 completely different characteristics from summer samples. The concentration of
195 EPFRs in fine particles (particle size $< 2.1 \mu\text{m}$) is $(1.8 - 3.6) \times 10^{14} \text{ spins}/\text{m}^3$, while the
196 concentration of EPFRs in coarse particles (particle size $> 2.1 \mu\text{m}$) is smaller than that
197 of fine particles, with values of $(1.0 - 2.1) \times 10^{14} \text{ spins}/\text{m}^3$. In addition, the
198 concentration of EPFRs in particulates $< 0.43 \mu\text{m}$ in winter is very high, but it is very
199 low in summer. According to the results of factor analysis in part 3.2 of this study, this
200 particulate matter is related to combustion, which indicates that coal combustion in
201 winter may provide an important contribution to EPFRs. The EPFR concentration in

202 the fine PM of Linfen reported above is equivalent to that in the fine PM of Xi'an, but
203 it is ten times smaller than that in the fine PM of Beijing (Yang et al., 2017; Chen et
204 al., 2019b). Although the particle size distribution characteristics of EPFRs in winter
205 and summer are different, their concentration levels are similar, which indicates that
206 the EPFR concentration is not related to the PM concentration, but is determined by
207 the source characteristics. The source characteristics will be discussed in detail in the
208 factor analysis section.

209 [Figure 1b shows the concentration ratio of EPFRs in coarse and fine particles](#)~~Figure~~
210 ~~1b shows the size-segregated contribution of EPFR concentration to the overall.~~ The
211 contribution of [EPFRs in](#) fine PM in summer is only 14.9%, while in winter is 58.5%.
212 The differences in EPFR concentrations with particle size may be related to the source
213 of EPFRs. For example, coarse particles are often associated with dust sources and
214 biogenic aerosols. In another study, the results have shown that dust particles contain
215 large amounts of metallic EPFRs and that they can be transported over long distances
216 (Chen et al., 2018b). EPFRs in fine particles may be mainly derived from the
217 combustion process, such as traffic sources, which are considered to be an important
218 source of EPFRs in atmospheric PM (Secrest et al., 2016; Chen et al., 2019b). Due to
219 winter heating in the Linfen area, the amount of coal burning increases sharply in this
220 season. In 2017, the nonclean heating (Coal-fired heating) rate of urban heating
221 energy structures in Linfen was 40% (data source: <http://www.linfen.gov.cn/>). With
222 the burning of coal, large amounts of EPFRs are produced, and in the summer, EPFRs
223 emitted by burning coal should be much less than those emitted in winter. This can
224 explain to a certain extent that the contribution of fine particles to summer EPFRs is
225 small, and the contribution of winter EPFRs is very large.

226 The g -factor obtained by using EPR to [analyze](#) the sample is an important
227 parameter to distinguish the type of EPFR. It is the ratio of the electronic magnetic
228 moment to its angular momentum (Shaltout et al., 2015; Arangio et al., 2016). The
229 g -factor of carbon-centered persistent free radicals is generally less than 2.003, the
230 g -factor of oxygen-centered persistent radicals is generally greater than 2.004, and the

231 g factor of carbon-centered radicals with adjacent oxygen atoms is between 2.003 and
232 2.004 (Cruz et al., 2012). Figure 2a shows the g-factor distribution characteristics of
233 EPFRs in different particle sizes in summer and winter. The g-factor of fine particles
234 and coarse particles shows different characteristics. The g-factor of EPFRs in fine
235 particles (particle size < 2.1 μm) ranges from 2.0034 to 2.0037, which may be from
236 carbon-centered radicals with adjacent oxygen atoms. However, the g-factor of
237 EPFRs in coarse particles (particle size > 2.1 μm) is significantly less than that of fine
238 particles. The g-factor ranges from 2.0031 to 2.0033, indicating that EPFRs in coarse
239 particles are more carbon-centered than those in fine particles and are free of
240 heteroatoms. As shown in Figure 2b, [the g-factor varied differently depending on](#)
241 [season](#). The g-factor of summer PM showed a significant decreasing trend with
242 increasing concentration, while the g-factor of winter PM showed a significant
243 increasing trend with increasing EPFR concentration. Oyana et al. (2017) studied
244 EPFRs in the surface dust of leaves in the Memphis region of the United States and
245 found that the concentration of EPFRs was positively correlated with the g-factor, and
246 they believed that this was related to the source of EPFRs. This phenomenon indicates
247 that the sources and toxicity of EPFRs in winter and summer are different.

248 3.2 Factor Analysis of EPFRs

249 To explore the possible sources and formation process of EPFRs in atmospheric
250 particles with different particle sizes, the NMF model was used to statistically analyze
251 EPFRs, carbon components, PAHs and metal elements in samples. The factors
252 obtained by the NMF model should reflect the different sources and generation
253 process of EPFRs. As shown in Figure 3a1 and b1, the three main contributing factors
254 to EPFRs in summer and winter are shown (see Figure S5, S6 for spectra of other
255 factors), which explain 94.5% and 83.8% of the EPFR concentrations in summer and
256 winter, respectively.

257 As shown in Figure 3a1, the typical spectral characteristic of summer factor 1 is
258 that it contains a small fraction of EC components and a large amount of OC
259 components, which indicates that combustion may be the source associated with this

260 factor. This factor has the highest loading of OC, especially WISOC; this fraction
261 mainly contains macromolecular organic substances, which are considered to
262 contribute to the main atmospheric particulate EPFRs and to be graphite oxide-like
263 substances (Chen et al., 2017; Chen et al., 2018a). Factor 2 is different from factor 1;
264 factor 2 is more likely the combustion of fossil fuels, while factor 1 should be other
265 combustion sources instead of burning coal, such as biomass combustion. The
266 generation process is similar to a hybrid process, which includes the graphite
267 oxide-like substances produced by incomplete combustion and the EPFRs formed by
268 some metal oxides. The typical characteristic of factor 3 is that the contribution of
269 metal elements is relatively high, while the contributions of EC and OC are very low.
270 Metal elements such as Al, Ti, Mn, and Co are typical crust elements, so this factor
271 may represent dust sources (Pan et al., 2013; Srivastava et al., 2007; Trapp et al.,
272 2010). The generation process of EPFRs. The others are likely derived from the
273 electroplating metallurgy industry (detailed in S1). As shown in Figure 3a2, the
274 contribution ratios of different factors show that the contribution ratios of factor 1 and
275 factor 2 are the highest, and factor 3 has only a small contribution, which indicates
276 that combustion sources, especially incomplete combustion, are the main sources of
277 EPFRs. The particle size distribution characteristics show that factor 1 is mainly
278 distributed in particles larger than 2.1 μm , while factor 2 is mainly distributed in
279 particles smaller than 0.43 μm .

280 The results of the factor analysis in winter are different from those in summer. As
281 shown in Figure 3b1, the typical spectral characteristic of factor 1 is that it contains a
282 large amount of OC components and As and Se. As and Se are trace elements of coal
283 combustion, as shown in many studies (Pan et al., 2013; Tian et al., 2010), so coal
284 combustion may be the source represented by this factor. From the generation process
285 viewpoint, the factor does not contain EC, but the content of OC is very high. In the
286 particles with a particle size of less than 3.3, which is mainly present in factor 1, the
287 concentration of OC is 16 times that of EC. So it may be mainly a graphite oxide-like
288 substance formed by the agglomeration of gaseous volatile organic compounds

289 (VOCs) generated during combustion. The typical spectral characteristics of factor 2
290 are due to a large amount of V and some Al, EC and OC. OC and EC are also typical
291 combustion products. V is rich in fossil fuels, especially fuel oil (Karnaev et al., 2011).
292 Therefore, traffic is the source represented by this factor. The factor contains crust
293 elements such as Al and Mn, so it is speculated that this factor may also include
294 traffic-related dust. The typical spectral characteristics of factor 3 are similar to those
295 of factor 1, and both contain relatively large amounts of As and Se, with the exception
296 that factor 3 contains a large amount of EC, indicating that it is also mainly derived
297 from incomplete combustion sources. The generation process of factor 3 should be
298 different from factor 1, which may include both the graphite oxide-like material
299 generated by fuel coking and the EPFRs generated by the metal oxide. The other
300 factors are mainly atmospheric dust and electroplating or metallurgy (see text S1). As
301 shown in Figure 3b2, factor 1 and factor 2 have the highest proportions, and factor 3
302 also has a small contribution, which indicates that winter is the same as summer, and
303 combustion sources are the main source of EPFRs. The particle size distribution
304 characteristics show that factor 1 is mainly distributed in particles with a size of 0.43 -
305 3.3 μm , while factor 2 is mainly distributed in particles larger than 3.3 μm .

306 Based on the above analysis, it can be found that combustion sources are the main
307 sources of EPFRs, and EPFRs from these sources are mainly graphite oxide-like
308 substances generated by the polymerization of organic matter or fuel coking. Studies
309 have shown that graphene oxide can cause cell damage by generating ROS (Seabra et
310 al., 2014). The surface of these compounds contains not only carbon atoms but also
311 some heteroatoms, which leads to disorder and the presence of defects in the
312 carbon-based structure (Lyu et al., 2018; Chen et al., 2017a; Mukome et al., 2013;
313 Keiluweit et al., 2010). The dust source is also a source of important EPFRs identified
314 in this study (with a contribution of approximately 10%). It was shown in the above
315 analysis that the concentration of EPFRs in coarse particles has a significant
316 correlation with the concentration of metallic elements, particularly crustal elements.
317 Some crustal elements, such as Al, and Fe, not only have their own paramagnetism

318 (Li et al., 2017; Yu et al., 2013; Nikitenko et al., 1992), but also interact with aromatic
319 compounds attached to the surface of the particles to produce a stable single-electron
320 structure.

321 3.3 Health risk of EPFRs

322 To evaluate the health risks of EPFRs in PM with different particle sizes, this study
323 evaluated the comprehensive exposure of EPFRs based on the deposition efficiency of
324 PM with different particle sizes in different parts of the human body. The results are
325 shown in Figure 4a. The ET region is the region with the highest EPFR exposure,
326 while the TB and P regions have relatively close EPFRs. This result shows that
327 atmospheric EPFRs are the most harmful to the health of the human upper respiratory
328 tract. Comparing the EPFR exposure in different seasons indicates that the exposure
329 risk in the ET area in summer is significantly higher than that in winter. This
330 difference occurs because the concentration of EPFRs in coarse particles is much
331 higher than that of fine particles in summer and the deposition efficiency of large
332 particles in the ET area is generally higher. Fine particles are more efficiently
333 deposited in the P region, leading to a higher risk of EPFR exposure in the P region in
334 winter.

335 EPFRs were found early in cigarette tar and are considered one of the health risk
336 factors in cigarette smoke (Lyons et al., 1960); thus, in this study, the exposure risks
337 of EPFRs in particles deposited in the human body were converted to the equivalent
338 number of cigarettes inhaled per adult per day. As shown in Figure 4b, the ET area is
339 the most contaminated area, with an average equivalence of twenty-one cigarettes
340 (twenty-five in summer and sixteen in winter). The average values for the TB area
341 (nine in summer and seven in winter) and P area (seven in summer and ten in winter)
342 are eight. The results indicate that EPFRs pose significant health risks to human lungs
343 in both winter and summer. Other similar studies, such as a study of the average
344 amount of EPFRs in PM_{2.5} inhaled per person per day in Xi'an in 2017, found values
345 equivalent to approximately 5 cigarettes (Chen et al., 2018a). Gehring and Dellinger
346 (2013) found that EPFR exposure in PM_{2.5} is equivalent to approximately 0.3

347 cigarettes per person per day in St. Joaquin County, the location with the worst air
348 pollution in the United States. The average exposure risk of EPFRs in fine particles in
349 the Linfen area (approximately 13 cigarettes) was higher than those in these two
350 studies. However, these previous studies only studied the exposure risk of EPFRs in
351 fine particles. The results of this study indicate that the health risks of EPFRs are
352 significantly increased when the particle size distribution of EPFRs is taken into
353 account. Therefore, it is important to study the source characteristics and generation
354 process of EPFRs with different particle sizes, which will be discussed in detail in the
355 following sections.

356 This study calculated the proportion of EPFRs with different particle sizes in
357 different parts of the respiratory system based on the deposition efficiency of particles
358 with different particle sizes. As shown in Figure 4c, in the ET region and the TB
359 region, coarse particles are the dominant component in summer and winter. In
360 particular, in summer, the proportion of EPFRs in coarse particles in these two regions
361 exceeds 95%. In the P region, there are significant differences between summer and
362 winter. The P region in summer is still dominated by coarse particles, but its
363 proportion is significantly lower than those in the ET and TB regions. In the P region
364 in winter, fine particles are the dominant component (approximately 70%). These
365 distribution characteristics indicate different sources of EPFRs in different regions. As
366 shown in Figure 4d, in summer, combustion sources are the main source of EPFRs in
367 the respiratory system. In winter, combustion and transportation sources contribute
368 equally in the EP and ET regions, while in the alveoli, combustion sources are the
369 main contributor. The ET region is the area with the highest risk of exposure to
370 EPFRs (21 cigarettes). The generation process of these EPFRs is mainly attributable
371 to graphene oxide-like substances. Studies have shown that graphene oxide is
372 cytotoxic (Harmon et al., 2018). In the alveoli, the contribution of combustion sources
373 is significantly increased (especially in winter). These EPFRs are mainly generated by
374 the action of metal oxides and organic substances. Studies have shown that such
375 EPFRs can generate ROS in the lung fluid environment (Khachatryan et al., 2011).

376 4. Conclusions and environmental implications

377 This study systematically reported the particle size distribution of EPFRs in
378 atmospheric PM in Linfen, which is one of the most polluted cities in China and is
379 located in a typical coal-burning area. In addition, this study evaluated the
380 comprehensive health risks of EPFRs, and reported possible sources and formation
381 process of atmospheric EPFRs with respect to different particle sizes. The following
382 main conclusions were obtained.

383 (1) This study found that EPFRs are widely present in atmospheric particles of
384 different particle sizes and exhibit significant particle size distribution characteristics.
385 The results of this study demonstrate that the concentrations and types of EPFRs are
386 dependent on particle size and season. This seasonal characteristic of EPFRs is mainly
387 affected by the PM sources, this result also indicates that the potential toxicity caused
388 by EPFRs may also vary with particle size and season.

389 (2) This study reported the possible source and formation process of atmospheric
390 EPFRs in different particle sizes. The results show that combustion is the most
391 important source of EPFRs (>70%) in both winter and summer PM samples in Linfen.
392 The graphite oxide-like process has the highest contribution (~70%) and is mainly
393 distributed in particles with a size of > 0.43 μm . These findings deepen our
394 understanding of the pollution characteristics of atmospheric EPFRs and are useful for
395 controlling EPFR generation in heavily polluted areas.

396 (3) This study assessed the exposure risk of EPFRs in different areas of the
397 respiratory system. The results show that the upper respiratory tract is the area with
398 the highest EPFR exposure. The trachea and alveoli are also exposed to EPFRs, and
399 the risk of exposure is equivalent to that of 8 cigarettes per person per day. Coarse
400 particles are the main source of EPFRs in the upper respiratory tract, while fine
401 particles are mainly involved in the alveoli.

402 Through this study, the results have shown that there are significant differences in
403 the concentrations and types of EPFRs in particles of different sizes and these
404 differences are due to the influence of the source and generation process. In the future,

405 assessments of the particle size distribution and the seasonality of EPFRs in
406 atmospheric PM should be considered. Health risks are another focus of this study. It
407 is found that the upper respiratory tract is the key exposure area of EPFRs, and the
408 traffic source is the main source of EPFRs in this area. This finding is significant for a
409 systematic assessment of the health risks of EPFRs. In view of the complexity and
410 diversity of the formation process of EPFRs in actual atmospheric particulates, the
411 relative contributions of EPFRs generated by different process and their associated
412 health risks should be more comprehensively studied in the future.

413 **Acknowledgments**

414 This work was supported by the National Natural Science Foundation of China
415 (grant numbers: 41877354, 41761144056 and 41703102), the Provincial Natural
416 Science Foundation of Jiangsu grant no. BK20180040), the Natural Science
417 Foundation of Shaanxi Province, China (2018JM4011) and the fund of Jiangsu
418 Innovation & Entrepreneurship Team.

419 **Appendix A. Supplementary data**

420 Appendix A contains additional details, including the EPR spectra of samples of
421 different particle sizes, correlations between EPFRs and carbon in particles of
422 different particle sizes, the results and errors of factor analysis, correlation analysis of
423 EPFRs with metallic elements, and EPFR exposure in different areas of the human
424 respiratory tract.

425 **Code/Data availability:** All data that support the findings of this study are
426 available in this article and its Supplement or from the corresponding author on
427 request.

428 **Author contribution:** Qingcai Chen: Research design, Methodology, Writing -
429 Original Draft, Writing - Review & Editing, Project administration, Funding
430 acquisition; Haoyao Sun: Investigation, Sample analysis, Writing - Original Draft,
431 Writing - Review & Editing, Methodology, Formal analysis; Wenhui Song:
432 Investigation, Sample collection, Chemical analysis; Fang Cao: Investigation, Sample

433 collection; Chongguo Tian: Investigation, Chemical analysis; Yan-Lin Zhang:
434 Conceptualization, Writing - Review & Editing, Formal analysis, Validation, Funding
435 acquisition.

436 **Competing interests:** The authors declare that they have no conflict of interest.

437 **References**

- 438 Arangio, A. M., Tong, H., Socorro, J., Pöschl, U., Shiraiwa, M., 2016. Quantification of
439 environmentally persistent free radicals and reactive oxygen species in atmospheric aerosol
440 particles. *Atmos. Chem. Phys.* 16 (20), 13105–13119.
- 441 Blakley, R. L., Henry, D. D., Smith, C. J., 2001. Lack of correlation between cigarette mainstream
442 smoke particulate phase radicals and hydroquinone yield. *Food. Chem. Toxicol.* 39 (4),
443 401–406.
- 444 Baum, S.L., Anderson, I.G.M., Baker, R.R., Murphy, D.M., Rowlands, C.C., 2003. Electron spin
445 resonance and spin trap investigation of free radicals in cigarette smoke: development of a
446 quantification procedure. *Anal. Chim. Acta* 481, 1–13.
- 447 Cruz, A.L.N.D., Cook, R.L., Lomnicki, S.M., Dellinger, B., 2012. Effect of low temperature
448 thermal treatment on soils contaminated with pentachlorophenol and environmentally
449 persistent free radicals. *Environ. Sci. Technol.* 46, 5971–5978.
- 450 Chen, N., Huang, Y., Hou, X., Ai, Z., Zhang, L., 2017. Photochemistry of hydrochar: Reactive
451 oxygen species generation and sulfadimidine degradation. *Environ. Sci. Technol.* 51 (19),
452 11278–11287.
- 453 Chen, Q., Mu, Z., Song, W., Wang, Y., Yang, Z., Zhang, L., Zhang, Y., 2019a. Size-resolved
454 characterization of the chromophores in atmospheric particulate matter in Linfen, China. *J.*
455 *Geophys. Res.-Atmos.* 124, DIO: 10.1029/2019JD031149.
- 456 Chen, Q., Ikemori, F., Nakamura Y., Vodicka, P., Kawamura, K., Mochida, M., 2017. Structural
457 and light-absorption characteristics of complex water-insoluble organic mixtures in urban
458 submicron aerosols. *Environ. Sci. Technol.* 51(15), 8293–8303.
- 459 Chen, Q., Miyazaki, Y., Kawamura, K., Matsumoto, K., Coburn, S., Volkamer, R., Iwamoto, Y.,
460 Kagami, S., Deng, Y., Ogawa, S., 2016. Characterization of chromophoric water-soluble
461 organic matter in urban, forest, and marine aerosols by HR-ToF-AMS analysis and
462 excitation–emission matrix spectroscopy. *Environ. Sci. Technol.* 50 (19), 10351–10360.
- 463 Chen, Q., Sun, H., Mu, Z., Wang, Y., Li, Y., Zhang, L., Wang, M., Zhang, Z., 2019b.
464 Characteristics of environmentally persistent free radicals in PM_{2.5}: Concentrations, species
465 and sources in Xi'an, Northwestern China. *Environ. Pollut.* 247, 18–26.
- 466 Chen, Q., Sun, H., Wang, J., Shan, M., Xue, J., Yang, X., Deng, M., Wang, Y., Zhang, L., 2019c.
467 Long-life type — The dominant fraction of EPFRs in combustion sources and ambient fine
468 particles in Xi'an. *Atmos. Environ.* 219, 117059.
- 469 Chen, Q., Sun, H., Wang, M., Mu, Z., Wang, Y., Li, Y., Wang, Y., Zhang, L., Zhang, Z., 2018a.
470 Dominant fraction of EPFRs from Nonsolvent-Extractable organic matter in fine particulates
471 over Xi'an, China. *Environ. Sci. Technol.* 52 (17), 9646–9655.

472 Chen, Q., Sun, H., Wang, M., Wang, Y., Zhang, L., Han, Y., 2019d. Environmentally persistent
473 free radical (EPFR) formation by visible-light illumination of the organic matter in
474 atmospheric particles. *Environ. Sci. Technol.*, 53 (17), 10053–10061.

475 Chen, Q., Wang, M., Sun, H., Wang, X., Wang, Y., Li, Y., Zhang, L., Mu, Z., 2018b. Enhanced
476 health risks from exposure to environmentally persistent free radicals and the oxidative stress
477 of PM_{2.5} from asian dust storms in erenhot, Zhangbei and Jinan, China. *Environ. Int.* 123,
478 260–268.

479 Chen, Q., Wang, M., Wang, Y., Zhang, L., Li, Y., Han, Y., 2019e. Oxidative potential of
480 water-soluble matter associated with chromophoric substances in PM_{2.5} over Xi'an, China.
481 *Environ. Sci. Technol.*, 53 (17), 10053–10061.

482 Chen, Q., Wang, M., Wang, Y., Zhang, L., Xue, J., Sun, H., Mu, Z., 2018c. Rapid determination of
483 environmentally persistent free radicals (EPFRs) in atmospheric particles with a quartz
484 sheet-based approach using electron paramagnetic resonance (EPR) spectroscopy. *Atmos.*
485 *Environ.* 184, 140–145.

486 Cheng, Y., He, K. B., Du, Z. Y., Engling, G., Liu, J. M., Ma, Y. L., Zheng, M., Weber, R. J., 2016.
487 The characteristics of brown carbon aerosol during winter in Beijing. *Atmos. Environ.* 127,
488 355–364.

489 Cormier, S. A., Lomnicki, S., Backes, W., Dellinger, B., 2006. Origin and health impacts of
490 emissions of toxic by-products and fine particles from combustion and thermal treatment of
491 hazardous wastes and materials. *Environ. Health. Perspect.* 114 (6), 810–817.

492 D'Arienzo, M., Gamba, L., Morazzoni, F., Cosention, U., Creco, C., Lasagni, M., Pitea, D., Moro,
493 G., Cepek, C., Butera, V., Sicilia, E., Russo, N., Muñoz-García, A., Pavone, M., 2017.
494 Experimental and theoretical investigation on the catalytic generation of environmentally
495 persistent free radicals from benzene. *J. Phys. Chem. A.* 121 (17), 9381–9393.

496 Dellinger, B., Lomnicki, S., Khachatryan, L., Maskos, Z., Hall, R. W., Adoukpe, J., McFerrin, C.,
497 Truong, H., 2007. Formation and stabilization of persistent free radicals. *Proc. Combust. Inst.*
498 31 (1), 521–528.

499 Dellinger, B., Pryor, W. A., Cueto, R., Squadrito, G. L., Hegde, V., Deutsch, W. A., 2001. Role of
500 free radicals in the toxicity of airborne fine particulate matter. *Chem. Res. Toxicol.* 14 (10),
501 1371–1377.

502 Environmental Protection Agency, 1988. Recommendations for and Documentation of Biological
503 Values for Use in Risk Assessment. PB-179874. EPA 600/6-87/008. US Environmental
504 Protection Agency, Cincinnati, OH.

505 Finkelstein, E., Rosen, G. M., Rauckman, E. J., 1982. Production of hydroxyl radical by
506 decomposition of superoxide spin-trapped adducts. *Mol. Pharmacol.* 21 (2), 262–265.

507 Gehling, W., Dellinger, B., 2013. Environmentally persistent free radicals and their lifetimes in
508 PM_{2.5}. *Environ. Sci. Technol.* 47 (15), 8172–8178.

509 Han, Y., Chen, Y. J., Saud, A., Feng, Y. L., Zhang, F., Song, W. H., Cao, F., Zhang, Y., Yang, X., Li,
510 J., Zhang, G., 2018. High time- and size-resolved measurements of PM and chemical
511 composition from coal combustion: Implications for the EC formation process. *Environ. Sci.*
512 *Technol.* 52 (11), 6676–6685.

513 Harmon, A. C., Hebert, V. Y., Cormier, S. A., Subramanian, B., Reed, J. R., Backes, W. L., Dugas,
514 T. R., 2018. Particulate matter containing environmentally persistent free radicals induces

515 AhR-dependent cytokine and reactive oxygen species production in human bronchial
516 epithelial cells. *Plos. One.* 13 (10), e0205412.

517 Karnae, S., John, K., 2011. Source apportionment of fine particulate matter measured in an
518 industrialized coastal urban area of South Texas. *Atmos. Environ.* 45 (23), 3769–3776.

519 Keiluweit, M., Nico, P. S., Johnson, M. G., Kleber, M., 2010. Dynamic molecular structure of
520 plant biomass-derived black carbon (biochar). *Environ. Sci. Technol.* 44 (4), 1247–1253.

521 Khachatryan, L., Dellinger, B., 2011. Environmentally persistent free radicals (EPFRs)-2. Are free
522 hydroxyl radicals generated in aqueous solutions?. *Environ. Sci. Technol.* 45 (21),
523 9232–9239.

524 Li, G. L., Wu, S. Y., Kuang, M. Q., Hu, X. F., Xu, Y. Q., 2017. Studies on the g-factors of the
525 copper(II)-oxygen compounds. *J. Struct. Chem.* 58 (4), 700–705.

526 Lin, P., Hu, M., Deng, Z., Slanina, J., Han, S., Kondo, Y., Takegawa, N., Miyazaki, Y., Zhao, Y.,
527 Sugimoto, N., 2009. Seasonal and diurnal variations of organic carbon in PM_{2.5} in Beijing
528 and the estimation of secondary organic carbon. *J. Geophys. Res.-Atmos.* 114, 1–41.

529 Liu, J., Bergin, M., Guo, H., King, L., Kotra, N., Edgerton, E., Weber, R. J., 2013. Size-resolved
530 measurements of brown carbon in water and methanol extracts and estimates of their
531 contribution to ambient fine-particle light absorption. *Atmos. Chem. Phys.* 13, 12389–12404.

532 Lomnicki, S., Truong, H., Vejerano, E., Dellinger, B., 2008. Copper oxide-based model of
533 persistent free radical formation on combustion-derived particulate matter. *Environ. Sci.*
534 *Technol.* 42 (13), 4982–4988.

535 Lyu, L., Yu, G., Zhang, L., Hu, C., Sun, Y., 2018. 4-Phenoxyphenol-functionalized reduced
536 graphene oxide nanosheets: A metal-free fenton-like catalyst for pollutant destruction.
537 *Environ. Sci. Technol.* 52 (2), 747–756.

538 Lyons, M.J., Spence, J.B., 1960. Environmental free radicals. *Br. J. Canc.* 14, 703–708

539 Mihara, T., Michihiro, M., 2011. Characterization of solvent-extractable organics in urban aerosols
540 based on mass spectrum analysis and hygroscopic growth measurement. *Environ. Sci.*
541 *Technol.* 45 (21), 9168–9174.

542 Mukome, F. N. D., Zhang, X., Silva, L. C. R., Six, J., Parikh, S. J., 2013. Use of Chemical and
543 physical characteristics to investigate trends in biochar feedstocks. *J. Agric. Food Chem.* 61
544 (9), 2196–2204.

545 Nikitenko, V. A., 1992. Luminescence and EPR of zinc oxide (review). *J. Appl. Spectrosc.* 57
546 (5–6), 783–798.

547 Oyana, T. J., Lomnicki, S. M., Guo, C., Cormier, S. A., 2017. A scalable field study protocol and
548 rationale for passive ambient air sampling: a spatial phytosampling for leaf data collection.
549 *Environ. Sci. Technol.* 51 (18), 10663–10673.

550 Pan, Y., Wang, Y., Sun, Y., Tian, S., Cheng, M., 2013. Size-resolved aerosol trace elements at a
551 rural mountainous site in Northern China: importance of regional transport. *Sci. total Environ.*
552 461–462, 761–771.

553 Patterson, M. C., Keilbart, N. D., Kiruri, L. W., Thibodeaux, C. A., Lomnicki, S., Kurtz, R. L.,
554 Poliakoff, E. D., Dellinger, B., Sprunger, P. T., 2013. EPFR formation from phenol adsorption
555 on Al₂O₃ and TiO₂: EPR and EELS studies. *Chem. Phys.* 422, 277–282.

556 Pryor, W.A., Prier, D.G., Church, D.F., 1983. Electron-spin resonance study of mainstream and
557 sidestream cigarette smoke: nature of the free radicals in gas-phase smoke and in cigarette tar.
558 *Environ. Health Perspect.* 47, 345–355.

559 Pryor, W. A., 1986. Oxy-Radicals and Related Species: Their Formation, Lifetimes, and Reactions.
560 *Annu. Rev. Physiol.* 48, 657–667.

561 Qi, L., Zhang, Y., Ma, Y., Chen, M., Ge, X., Ma, Y., Zheng, J., Wang, Z., Li, S., 2016. Source
562 identification of trace elements in the atmosphere during the second Asian Youth Games in
563 Nanjing, China: Influence of control measures on air quality. *Atmos. Pollut. Res.* 7, 547–556.

564 Shaltout, A. A., Boman, J., Shehadeh, Z. F., Al-Malawi, D. A. R., Hemeda, O. M., Morsy, M. M.,
565 2015. Spectroscopic investigation of PM_{2.5}, collected at industrial, residential and traffic
566 sites in taif. Saudi Arabia. *J. Aerosol. Sci.* 79, 97–108.

567 [Song, W., Cao F., Lin Y., Haque, M. M., Wu, X., Zhang, Y., Zhang, C., Xie, F., Zhang Y., 2020.](#)
568 [Extremely high abundance of polycyclic aromatic hydrocarbons in aerosols from a typical](#)
569 [coal-combustion rural site in China: Size distribution, source identification and cancer risk](#)
570 [assessment. *Atmos. Res.* 248, 105192.](#)

571 Srivastava, A., Jain, V. K., 2007. Size distribution and source identification of total suspended
572 particulate matter and associated heavy metals in the urban atmosphere of Delhi.
573 *Chemosphere.* 68(3), 579–589.

574 Strak, M., Janssen, N. A. H., Godri, K. J., Gosens, I., Mudway, I. S., Cassee, F. R., Lebret, E.,
575 Kelly F. J., Harrison, R. M., Brunekreef, B., Steenhof, M., Hoek, G., 2012. Respiratory health
576 effects of airborne particulate matter: The role of particle size, composition, and oxidative
577 potential—the RAPTES project. *Eviron. Health. Persp.* 120 (8), 1183–1189.

578 Salma, I., Balásházy, I., Winkler-Heil, R., Hofmann, W., Zárny, G. 2002. Effect of particle mass
579 size distribution on the deposition of aerosols in the human respiratory tract. *J. Aerosol. Sci.*
580 33(1), 119-132.

581 Seabra A.B., Paula A.J., Lima R. D., Alves. O.L., Durán. N. 2014. Nanotoxicity of graphene and
582 graphene oxide. *Chem. Res. Toxicol.* 27 (2), 159–168.

583 Thevenot, P. T., Saravia, J., Jin, N., Giaimo, J. D., Chustz, R. E., Mahne, S., Kelley, M. A., Hebert,
584 V. Y., Dellinger, B., Dugas, T. R., Demayo, F. G., Cormier, S. A., 2013. Radical-containing
585 ultrafine particulate matter initiates epithelial-to-mesenchymal transitions in airway epithelial
586 cells. *Am. J. Respir. Cell. Mol. Biol.* 48 (2), 188–197.

587 Tian, H., Wang, Y., Xue, Z., Cheng, K., Qu, Y., Chai, F., Hao, J., 2010. Trend and characteristics of
588 atmospheric emissions of Hg, As, and Se from coal combustion in China, 1980–2007. *Atmos.*
589 *Chem. Phys.* 10 (23), 11905–11919.

590 Tong, H., Lakey, P. S. J., Arangio, A. M., Socorro, J., Shen, F., Lucas, K., Brune, W. H., Pöschl,
591 U., Shiraiwa, M., 2018. Reactive oxygen species formed by secondary organic aerosols in
592 water and surrogate lung fluid. *Environ. Sci. Technol.* 52 (20), 11642–11651.

593 Trapp, J. M., Millero, F. J., Prospero, J. M., 2010. Temporal variability of the elemental
594 composition of African dust measured in trade wind aerosols at Barbados and Miami. *Mar.*
595 *Chem.* 120 (1-4), 71–82.

596 Truong, H., Lomnicki, S., Dellinger, B., 2010. Potential for misidentification of environmentally
597 persistent free radicals as molecular pollutants in particulate matter. *Environ. Sci. Technol.* 44
598 (6), 1933–1939.

599 Valavanidis, A., Fiotakis, K., Vlachogianni, T., 2008. Airborne particulate matter and human health:
600 toxicological assessment and importance of size and composition of particles for oxidative
601 damage and carcinogenic mechanisms. *J. Environ. Sci. Heal. C.* 26 (4), 339–362.

602 Vejerano, E. P., Rao, G., Khachatryan, L., Cormier, S. A., Lomnicki, S., 2018. Environmentally
603 persistent free radicals: Insights on a new class of pollutants. *Environ. Sci. Technol.* 52 (5),
604 2468–2481.

605 Vejerano, E., Lomnicki, S. M., Dellinger, B., 2012a. Formation and stabilization of
606 combustion-generated, environmentally persistent radicals on Ni(II)O supported on a silica
607 surface. *Environ. Sci. Technol.* 46 (17), 9406–9411.

608 Vejerano, E., Lomnicki, S., Dellinger, B., 2011. Formation and stabilization of
609 combustion-generated environmentally persistent free radicals on an Fe(III)2O3/silica surface.
610 *Environ. Sci. Technol.* 45 (2), 589–594.

611 Valavanidis, A., Haralambous, E., 2001. A comparative study by electron paramagnetic resonance
612 of free radical species in the mainstream and sidestream smoke of cigarettes with
613 conventional acetate filters and 'bio-filters. *Redox. Rep.* 6, 161–171.

614 Vejerano, E., Lomnicki, S., Dellinger, B., 2010. Formation and stabilization of
615 combustion-generated environmentally persistent free radicals on an Fe(III) 2O3/silica
616 surface. *Environ. Sci. Technol.* 45 (2), 589–594.

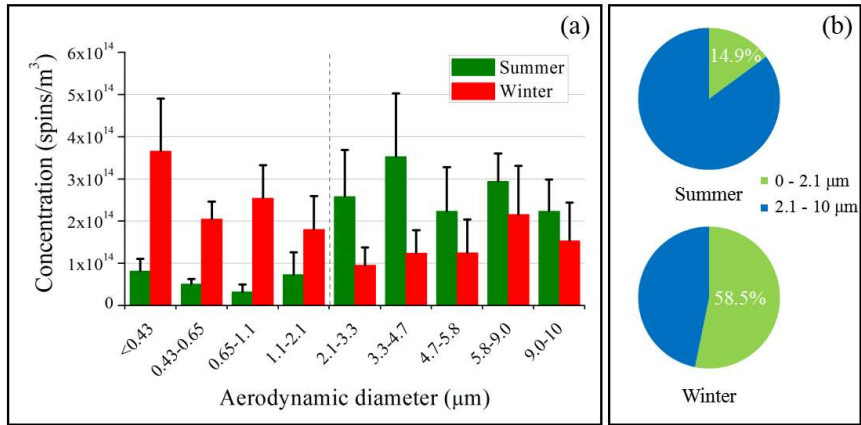
617 Vejerano, E., Lomnicki, S., Dellinger, B., 2012b. Lifetime of combustion-generated
618 environmentally persistent free radicals on Zn(II)O and other transition metal oxides. *J.*
619 *Environ. Monit.* 14 (10), 2803–2806.

620 Wang, P., Pan, B., Li, H., Huang, Y., Dong, X., Fang, A., Liu, L., Wu, Min., Xing, B., 2018. The
621 overlooked occurrence of environmentally persistent free radicals in an area with low-rank
622 coal burning, Xuanwei, China. *Environ. Sci. Technol.* 52 (3), 1054–1061.

623 Wang, Y., Li, S., Wang, M., Sun, H., Mu, Z., Zhang, L., Li, Y., Chen, Q., 2019. Source
624 apportionment of environmentally persistent free radicals (EPFRs) in PM2.5 over Xi'an,
625 China. *Sci. Total. Environ.* 689, 193–202.

626 Yang, L., Liu, G., Zheng, M., Jin, R., Zhu, Q., Zhao, Y., Wu, X., Yang, X., 2017. Highly elevated
627 levels and particle-size distributions of environmentally persistent free radicals in
628 haze-associated atmosphere. *Environ. Sci. Technol.* 51 (14), 7936–7944.

629 Yu, T., Wang, J., Shen, M., Li, W., 2013. NH3-SCR over Cu/SAPO-34 catalysts with various acid
630 contents and low Cu loading. *Catal. Sci. Technol.* 3 (12), 3234–3241.

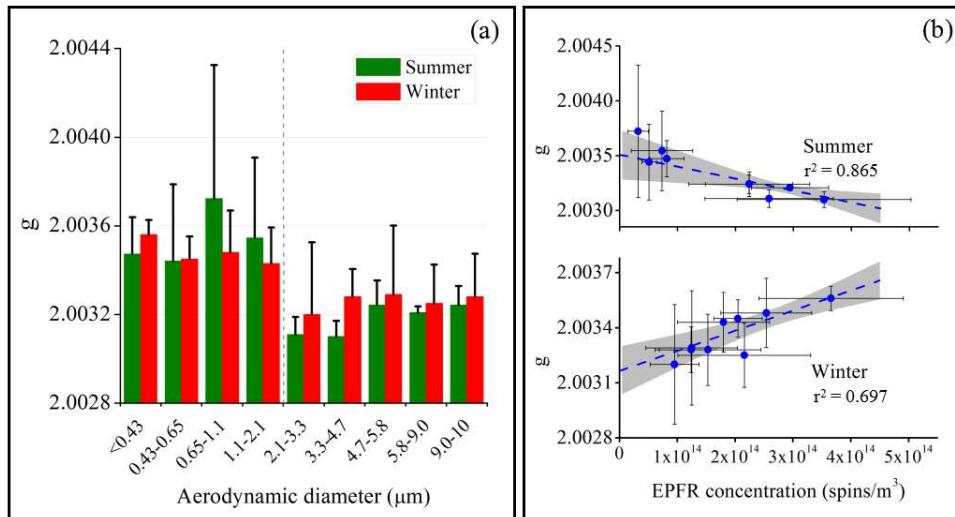


631

632 Figure 1. The concentration of EPFRs in PM with different particle sizes. (a) Atmospheric

633 concentrations of EPFRs in different particle sizes in summer and winter. (b) The relative

634 contribution of fine particles and coarse particles to the total EPFR concentration.

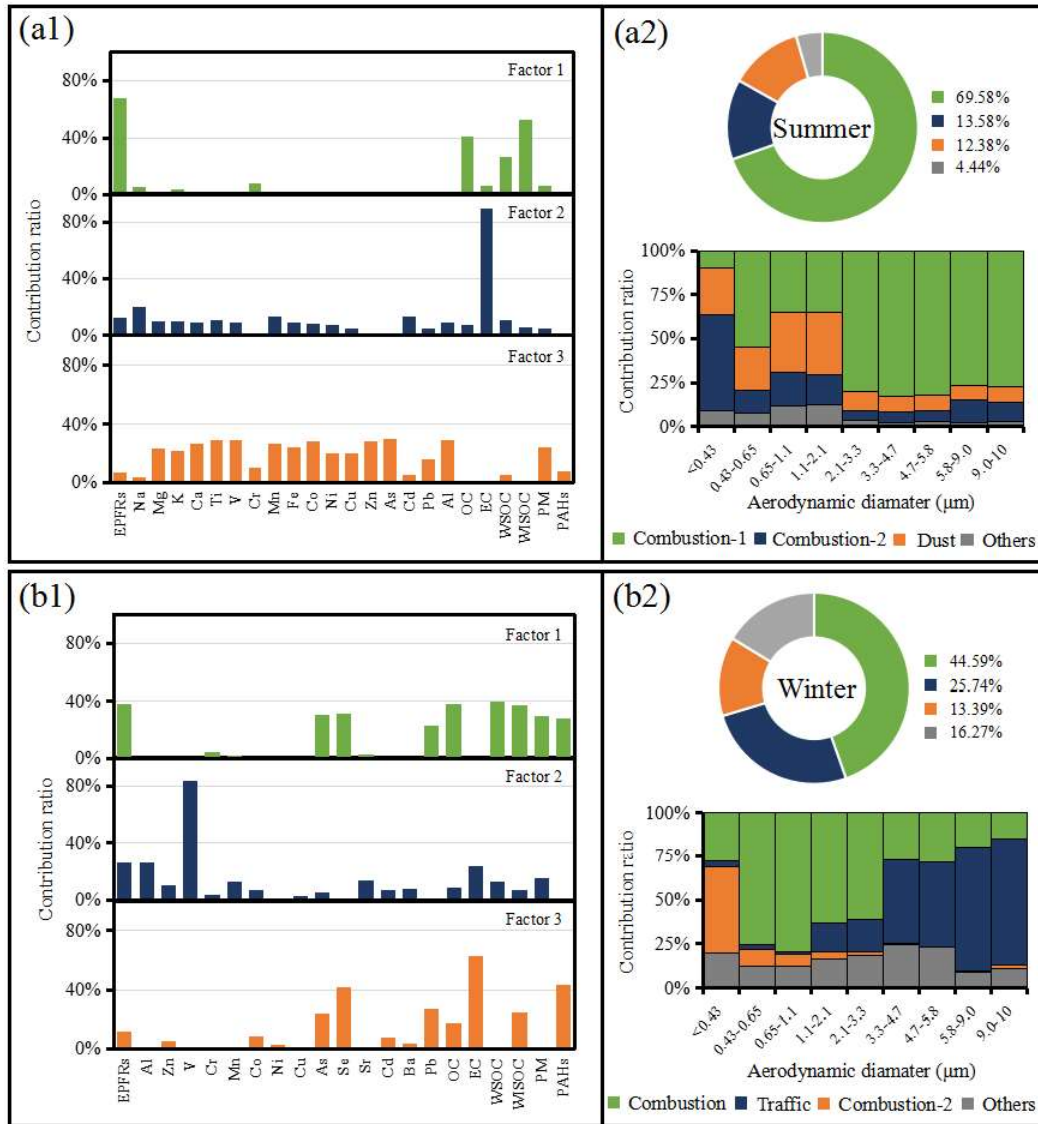


635

636 Figure 2. A g -factor comparison. (a) Comparison of g -factors of EPFRs in different particle sizes

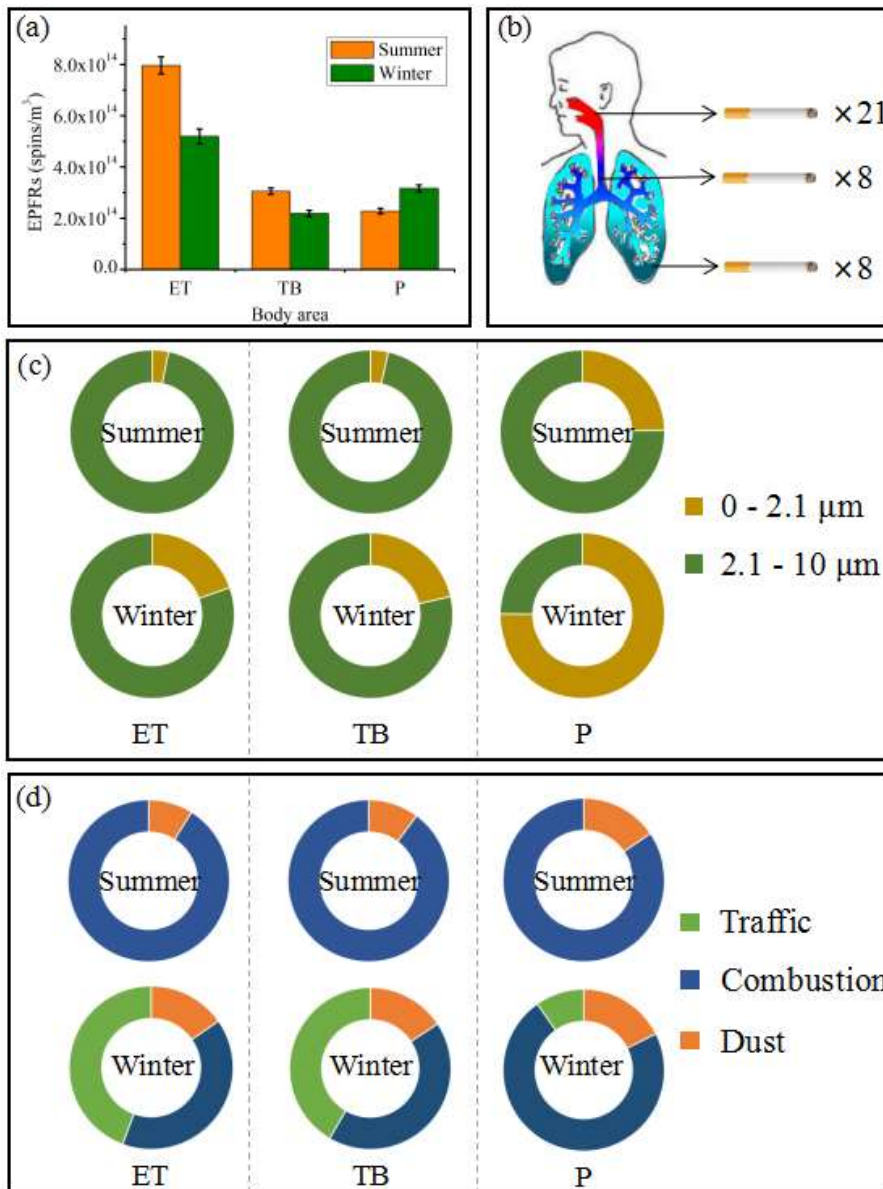
637 in different seasons. (b) Correlation analysis of g -factors and concentrations of EPFRs in summer

638 and winter PM. The gray areas in the figure represent 95% confidence intervals.



639

640 Figure 3. Factor analysis of EPFRs in different particle sizes in different seasons. (a1) and (b1)
 641 represent the results of factor analysis for summer and winter, respectively. (a2) and (b2) represent
 642 the contribution of various factors in summer and winter, respectively, to EPFRs and the relative
 643 contributions of each factor for different particle sizes.



644

645 Figure 4. Exposure risks to EPFRs. (a) EPFR exposure in the ET, TB, and P regions. (b) Cigarette

646 exposure to EPFRs in the human respiratory system. (c) Exposure ratio of EPFRs with different

647 particle sizes in different areas of the respiratory system. (d) Contribution of EPFRs from different

648 sources to different areas of the respiratory system.